LAUTECH Journal of Engineering and Technology 17 (2) 2023: 83-103

OPTIMIZATION AND MODELLING OF BIO-OIL YIELD FROM THE PYROLYSIS OF *JATROPHA CURCAS* SEED USING OPTIMAL DESIGN AND ARTIFICIAL NEURAL NETWORKS

[1, 2*]Oladosu K. O., [3]Amoloye T. O., [4]Mustapha K., [1]Oderinde J. O., [5]Babalola S.

[1]*Department of Mechanical Engineering, Kwara State University, Malete, Nigeria*
[2]*Center for Sustainable Energy, Kwara State University, Malete, Nigeria*
[3]*Department of Aeronautical and Astronautical Engineering, Kwara State University, Malete, Nigeria*
[4]*Department of Material Science and Engineering, Kwara State University, Malete, Nigeria*
[5]*CSIR-Central Mechanical Engineering Research Institute (CMERI), Durgapur, West Bengal, India.*
***Corresponding author**: kamoru.oladosu@kwasu.edu.ng*

ABSTRACT

Better quality and quantity of pyrolysis products from biomass can be obtained by regulating the input parameters of the pyrolysis process. Pyrolysis of Jatropha Curcas seed mixed with alumina catalyst was carried out in a fixed bed reactor to study the effects of temperature, time, and particle size on bio char and bio-oil yield. The bio-oil yields were optimized using the Optimal Design (OD) under the Combined Methodology of the Design-Expert Software (12.0). The input and output parameters were modeled and validated using Artificial Neural Networks (ANN) based on 40 experimental data generated by the OD. The optimum bio-oil yield of 15.6 wt. % was obtained at 650 °C, 30 min, and 1 mm particle size. The Correlation Coefficient (R^2) of the model for the bio-char and bio-oil yield under the OD were 0.998 and 0.996, respectively. The optimized ANN architecture employed the in-built Levenberg-Marquardt training algorithm in MATLAB software. Random division of the data into training, validation and testing sets followed 70:15:15 percentage proportions with 15 hidden layers. This resulted in the minimum Mean Square Error (MSE) of 2.15e-05 and (R^2) of 0.96394 for the bio-oil yield. The FTIR spectra indicated that bio-oil contained phenols, esters, and acids compound while its Gas Chromatography analysis showed the presence of pyrrolidine, pyrimidine, and aldehydes. These properties signified the bioenergy and biochemical capabilities of the pyrolytic oil obtained. The prediction accuracy indicates that both the ANN and OD can be deployed for accurate prediction.

Keywords: *ANN, Bio-oil, Catalyst, Jatropha Caucus, Optimal Design, Pyrolysis*

INTRODUCTION

The increase in the global population coupled with the growth of the automobile industry among others has led to the depletion of fossil fuels and a consequent rise in the price of petroleum products in the past few decades (Tian et. al., 2020). Furthermore, the exploration of fossil fuels and the applications of their products is partly responsible for the increase in carbon dioxide (CO_2), depletion of the ozone layer, and general environmental pollution. Consequently, the development of alternative renewable and eco-friendly alternative energy sources is *sine-qua-non* (Lewis and Fletcher 2013, David et. al., 2018, and Adeniyi et. al., 2021). Biomass, which accounts for about 14% of the world's energy consumption and one-quarter of energy sources, appears to be a potential alternative (Kumar et. al., 2019). Agricultural residues can be used as biomass fuel for commercial heating and this subsequently reduces environmental pollution (Arulprakasajothi et. al., 2020). Biomass is derived from lignocellulose-contained plants such as Jatropha which is a shrub native to Brazil but now planted in Mali, Nigeria, Senegal, and Cote d'Ivoire

(Kanaujia et. al., 2016). Jatropha fruit contains 30-40% of oil and this makes it suitable for the production of industrial chemicals and biodiesel. However, oils produced from jatropha fruits have a higher viscosity, lower volatility, and reactivity in contrast to normal oils because of the attendance of unsaturated hydrocarbon chains (Boubacar et. al., 2020 and Kethobile et. al., 2020).

Oils are extracted from biomass via a thermochemical conversion process which includes pyrolysis, combustion, carbonization, liquefaction, and gasification (Kethobile et. al., 2020 and Oladosu et. al., 2021). Pyrolysis involves the transformation of biomass to char, oil, and non-condensable gas under the influence of heating rate, nitrogen flow rate, residence time, temperature, and particle size. Char components can be applied as fertilizers and steam power plants owing to their high heating value. Pyrolysis oil, a brownish organic liquid fuel that may be considered as feedstock in the creation of better-quality chemicals for the automobile industry, fuel in furnaces, boilers and superheater tubes for steam production while the gaseous products can be utilized as an alternative for biogas and natural gas for electricity generation (Okonkwo et. al., 2018).

Pyrolysis oil emerges from the complex mixture of water (15 to 30%) and various oxygen-containing compounds (28 to 40%) such as hydroxyl ketones, hydroxyl aldehydes, esters, furans, sugars, phenols, and carboxylic acid (Ndukwu et. al., 2020). Because of their oxygen-rich composition, bio-oils have low heating values and high viscosity. They are chemically unstable and immiscible with hydrocarbons (Rahman et. al., 2020). Consequently, increasing stability, calorific value, and lowering the viscosity are necessary. This can be done by reducing the quantity of oxygenated compounds via the breaking down of complex hydrocarbons into simpler molecules by the use of catalysts such as mesoporous materials, aluminium oxide, calcium oxide, zinc oxide, and zeolites (Ahmad et. al., 2018 and Wang et. al., 2020).

Sunarno et al. (2018) reported that the amorphous $SiO\text{-}Al_2O_3$ catalyst has a larger pore volume than the zeolite catalyst. The lignin macromolecules or dimeric in between $SiO\text{-}Al_2O_3$ could spread into these pores thereby making the catalyst engaged in either primary or secondary degradation reactions. At higher temperatures, the oil yield induced by the $SiO\text{-}Al_2O_3$ catalyst reduced whereas the gas yield increased. Kumar et al., (2019) stated that for the thermal decomposition of sewage sludge with composite alumina in a fixed bed pyrolytic unit at the temperature range of 400 - 650 ^oC, the non-condensable gas, liquid, and char yield depends on the temperature change. It was acknowledged that at a temperature of 500 ^oC, the maximum liquid and usable energy yield were 48.44wt% and 3871kJ/kg respectively with a mass ratio of 1/5 composite alumina/sewage sludge. Mishra et al., (2020) reported optimum process conditions and thermal decomposition of cascabel seeds, it was deduced that maximum bio-oil (45.26 wt.%) was obtained at the temperature of 525 °C, the flow rate of 75 mL/min for the nitrogen gas, and rate of heating of 75 °C/min whereas with the presence of CaO catalysts at 20 wt.% the bio-oil yield increased to 49.12wt.%. Yusuff and Owolabi (2019) characterized alumina-supported coconut chaff catalyst for the production of biodiesel. The outcome of the study shows that a reaction time of 150 mins, a temperature of 338K, catalyst loading of 1.5 wt.% and a methanol molar ratio of 12:1, produced biodiesel (91.05 wt.%). Garba et al. (2018) reported Catalytic upgrading of pyrolytic oil using bagasse as a biomass feedstock, it was noted that at a temperature of 500 °C and 15% zeolite catalyst, the maximum bio-oil yield with and without catalyst was 49.4% and 21.1 wt.%

respectively. Since the characteristics of bio-oil largely depend on the complex interaction between the processing parameters/factors, it is therefore important to predict and maximize these characteristics by using available tools such as Artificial Neural Networks (ANN).

ANN has been deployed for the optimization and prediction of biomass pyrolysis products such as non-oil jatropha caucus (Kethobile et. al., 2020), waste pomegranate peel (Siddiqui et. al., 2019), sugarcane bagasse (Kanwal et. al., 2019), palm kernel shell (Ozonoh et. al., 2020), perennial grass (Mishra et. al., 2020), breadfruit starch hydrolysate (Eriola and Ezekiel, 2015), birch branches (Bach and Lee, 2017), coal (Ahmad et. al., 2019) and Acacia nilotica (Singh et. al., 2020) among others. However, there is no report on the optimization and prediction of bio-oil yield from the pyrolysis of *Jatropha Curcas* seed blends with alumina catalyst through OD and ANN-based approach. This study, therefore, aims at investigating the process modeling, optimization, and prediction of bio-oil yield from *Jatropha Curcas* seed - alumina mixture which is a necessity for industrial process scale-up.

SAMPLE PROCUREMENT AND PREPARATION

Jatropha Caucus seed was obtained at Osin Budo-Are in Ilorin, Kwara State, Nigeria. The plant materials were dried outdoor, sieved into various particle sizes (1-3 mm) using a biomass mill grinder (SG-16 Series), and then taken to the laboratory for various analyses. Proximate analysis was conducted, under ASTM standards (E 871–82), to examine the properties of the biomass. The percentage compositions of the carbon (C), sulphur (S), and nitrogen (N) contents of the samples were evaluated using the elemental analyser CHNS-932 (LECO). A commercial-grade Alumina with maximum limits of impurities water-insoluble matter (0.2%), loss on ignition at 1100 ^{o}C (0.5%) Chloride Cl (0.005%). Sulphate (SO_4) and Iron Fe (0.005) was obtained from reliable representatives of the manufacturer and were chosen because of their capability to improve the quality of bio-oil yield and remove oxygenated compounds. To improve the alumina substance, it was cachinnated at 450 ^{o}C for 1hr and earmarked in a desiccator to avoid moisture absorption. The FTIR analysis was done to classify the presence of the functional group of biomass while GC examination was conducted on the optimized bio-oil yield to determine the compounds present in the extracted oil.

EXPERIMENTAL DESIGN

Experimental design involves the selection of the minimum number of design parameters and experimental trials to build the most accurate regression models. The techniques are generally based on Euclidean space, Borel set, and Caratheodory's theorem. Theoretical details are presented elsewhere (Jeirani et. al., 2012). For the current study, experiments were designed and optimized using Design-Expert version 12 within the ranges of the process mixture (*Jatropha Curcas* seed (JAS) and alumina catalyst) and factors (temperature, time, and size of the particle) as shown in Table 1. The nitrogen gas flow rate (75mL/min) was kept constant (Mth and Mubarak, 2019).

EXPERIMENTAL APPARATUS AND OPERATION

The pyrolysis tests were done using a fabricated fixed bed reactor in a nitrogen-rich environment (Fig. 1). The pyrolysis unit comprises a stainless steel vertical fixed bed reactor (5 cm in width, and length 65 cm) with a distribution plate of 1.0 mm diameter placed inside the heating element at 8 cm from the bottom (Fig. 1).

Table 1. Minimum and maximum values of experimental parameters

Levels	Component Mixture		Factors		
	JAS (wt.%)	Alumina (wt.%)	Temperature (ºC)	Particle (mm)	Time (min)
Minimum value	90	0	450	1	15
Maximum value	100	10	650	3	30

JAS-*Jatropha Curcas* seed

The biomass samples were mixed with the catalyst and placed in the retort in preparation for pyrolysis. For each experimental run, the reactor temperature was set to 30 ºC higher than the desired temperature to compensate for the heat absorbed by the retort and heat loss by convection (Mishra et. al., 2020). The samples were thereafter heated steadily under nitrogen gas (Guedes et. al., 2018). The spiral condenser barrel dipped in the ice salt bath was linked to the reactor to condense the vapour while a gas sample bag was used for the non-condensable gases. The char was taken out of the reactor after the specified resident time, air-cooled, and then measured. Similarly, the bio-oil was measured after condensation. This procedure was followed for all biomass samples at different heating times and pyrolysis temperatures according to each experimental run. After each experiment, the product yields were evaluated according to Equations 1-3 (Siddiqui et. al., 2019 and Kamoru et. al., 2024).

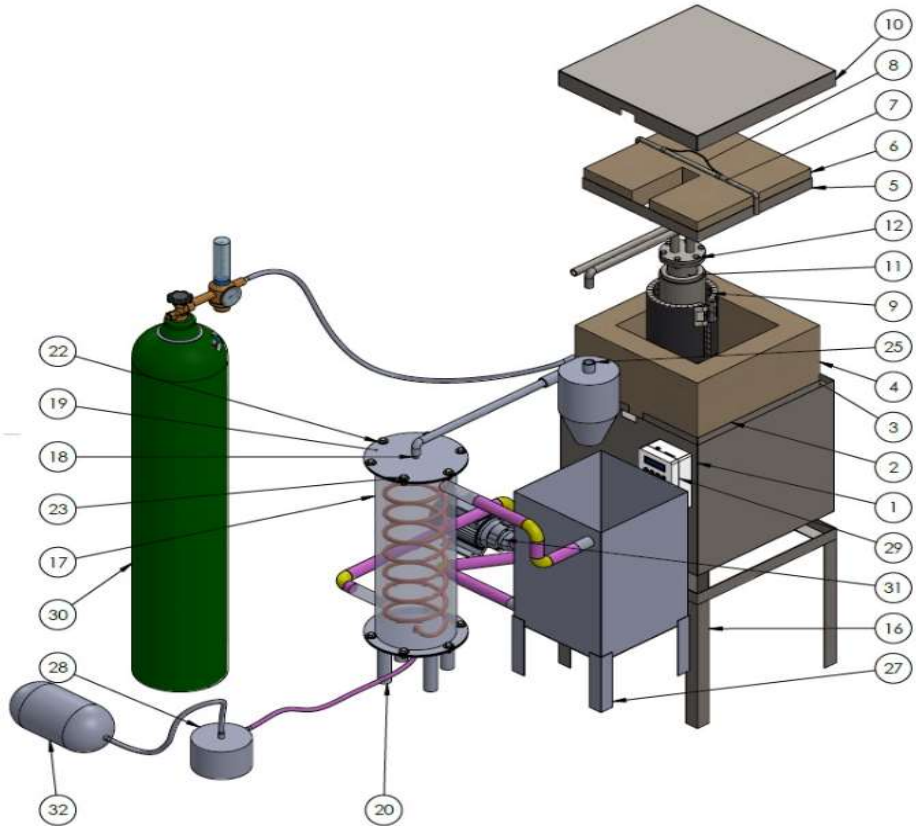

Fig. 1. Fixed bed pyrolytic unit

Item	Part list	Qty	Item	Part list	Qty
1	Combustion chamber enclosure	**1**	17	Condenser barrel	1
2	Combustion chamber enclosure	1	18	Condenser coil	1
3	Inter enclosure cover	1	19	Top condenser lid	1
4	Refractory bricks	Lot	20	Bottom condenser welded	1
5	Top refractory bricks frame	-	21	Condenser gasket	1
6	Combustion chamber top refractory	1	22	B 18.22m plain washer narrow	12
7	Top refractory frame hang	1	23	B 18. 2.3.2 m hex-screw M10 x 1.5 x 25-25 CN	12
8	Top refractory handle	1	24	B 18. 22.4 m Hex flange nut M 10 x1.5 with 15 WAF N	12
9	Heating element	1	25	Cyclone	1
10	Combustion chamber lid	1	26	Biomass piping	1
11	Reactor	1	27	Biomass water tank	1
12	Reactor lid	1	28	Bio oil collector	1
13	Reactor gasket	1	29	Custom control box	1
14	B 18.6.7m-m8x1.25x30 indented	1	30	Nitrogen gas cylinder	1
15	B 18.2.24M Hex flange nut M8x 1.25N	6	31	0.5hp water pump	1
16	Combustion chamber stand	1	32	Gas bag	1

%Char yield =

$$\frac{Mass\ of\ the\ char\ obtained\ after\ pyrolysis}{Mass\ of\ the\ dried\ raw\ biomass} \times 100\% \quad (1)$$

% Bio-oil yield =

$$\frac{Mass\ of\ the\ liquid\ obtained\ after\ pyrolysis}{Mass\ of\ the\ dried\ raw\ biomass} \times 100\% \quad (2)$$

% Gas yield = 100 – (Bio-oil yield % + Char yield %) (3)

GAS CHROMATOGRAPHY ANALYSIS OF BIO-OIL

The chemical components were separated with Agilent 6890 gas chromatograph equipped with an on-column automatic injector, flame ionization detector, and HP 88 capillary column (100 m x 0.25 µm film thickness) (made in the USA). The temperature of the gas chromatographer column was initially set at 160 °C for 2 mins, increased to 180 °C at 6 °C/min, maintained for 2 mins at 180 °C, then further increased to 230 °C at 4 °C/ min, and finally maintained for 10 min at 230 °C. The temperature of 230 and 250 ^{0}C was maintained for the injector and detector while the split ratio was 50:1

PHYSICOCHEMICAL PROPERTIES OF BIO-OIL

The calorific value and viscosity of the pyrolytic oil were measured with an oxygen bomb calorimeter (XRY-1A Oxygen bomb calorimeter) and a rotational viscometer. Furthermore, the moisture content and acidity were estimated by the Karl Fischer water analyser and Eutech water-resistant pH meter, respectively (Boubacar et. al., 2020 and Kareem et. al., 2018).

ANN MODELLING OF PYROLYSIS PROCESS

Artificial neural networks are efficient data-driven modelling tools widely used for non-linear

modelling and identification, consisting of input layers, hidden layers and output layers linked to each other by adjustable weight and bias. In the present study, input layers were based on five parameters such as JAS, Alumina, temperature, particle size and time while the output layer was bio-oil yield. The modelling was performed in MATLAB software through a multilayer perceptron feed-forward network trained with Levenberg-Marquardt training algorithm, *trainlm*. The 40 experimental data generated by OD were randomly divided into three groups: training data (70%), validation data (15%) and testing data sets (15%) for the bio-oil yield. Several hidden layers were tested because the ANN model with a single layer is often too feeble for accurate prediction of a non-linear function (Asafa et. al., 2013). In addition, the prediction accuracy of the models was also a function of the selected training algorithm. Antwi et al. (2017) stated that "*trainbfg*" and "*traincgb*" did excellently when matched with other eight trained algorithms for the prediction of methane and biogas yields. Though Chukwuneke et al. (2021) ranked '*trainlm*' best for the prediction of biochar, bio-oil and condensable gases from the pyrolysis of industrial biomass wastes. Conversely, Oladosu et al. (2021) observed "*trainscg*'' as the best algorithm for the prediction of combustion characteristics of palm fruit biomass in a grate furnace. The preceding shows that the selection of the algorithm hinges on the obtainable data or problem definition. Therefore, the best algorithm can be chosen through an optimized ANN architecture.

VERIFICATION OF ESTIMATED DATA

Mean Square Error (MSE), and Correlation Coefficients (R^2) were used to evaluate the ANN architecture. These are common measures for model predictability are determined from Equations 4 and 5 respectively.

$$MSE = \frac{1}{n}\sum_{i=1}^{n}(y_i - y_{ai})^2 \quad (4)$$

$$R^2 = 1 - \frac{1}{n}\sum_{i=1}^{n}\frac{(y_i - y_{ai})^2}{(y_{ai} - y_{mi})^2} \quad (5)$$

where n is the number of points, y_i is the predicted value obtained from the neural network, y_{ai} is the actual value and y_{mi} is the average of actual value.

The network having minimum MSE and maximum R^2 is considered the best. R^2 values that are close to a value of 1.0 indicate very agreeable accuracy of the model (Eriola and Ezekiel, 2015).

RESULTS AND DISCUSSION

Physicochemical properties of raw JAS

The proximate analysis of the JAS showed the attendance of volatile matter (66.31%), fixed carbon (15.75%), moisture content (4.28%), and ash content (11.54%) (Table 2). The higher percentage of volatile matter made biomass more attractive as a pyrolysis feedstock (Mishra and Mohanty, 2020). According to the elemental analysis, the feedstock contained carbon (43.37%), hydrogen (5.19%), nitrogen (1.53), sulphur (0.01%), and oxygen (49.53%) which is similar to a previously reported study (Siddiqui et. al., 2019). This brings to bear the vital elements that influence energy value and emission. In addition, JAS was rich in lignin (35.67 %), cellulose (26.12 wt. %), and hemicellulose (19.35%).

Optimal Design and Statistical Analysis

Table 3 contains 40 experimental runs obtained from the OD along with their respective bio-char and oil yields. Regression analysis was conducted to establish the relationship between the dependent variables (char and oil yields) and independent variables (temperature, time, and particle size). The relationships, as presented in Eq. (6) and (7), were also evaluated for accuracy and sufficiency using analysis of variance (ANOVA).

Table 2. Proximate, ultimate, and fiber analysis of feedstock

Analysis	Component	Composition (wt. %)
Proximate	Moisture	4.28
	Ash	11.54
	Fixed Carbon	15.75
	Volatile Matter	66.31
Ultimate	Carbon	43.37
	Oxygen	49.53
	Hydrogen	5.19
	Nitrogen	1.53
	Sulphur	0.01
Fiber	Hemicellulose	19.35
	Cellulose	26.12
	Lignin	35.67

Char yield = $+20.30A + 29.19B + 3.23AD + 4.94AD + 1.17BD - 0.992BE + 15.98\,ABE - 154ACD + 2.42ACE + 1.69BCD + 0.9484BDE + 20.30A + 6.34\,AD^2 + 3.94\,AE^2 + 2.00BC^2 - 1.38BE^2 - 4.83ABCD + ABDE$ (6)

Bio-Oil yield = $+5.25AE + 3.84B - 9.66AB + 1.24AE + 3.20BC + 2.18BE + 1.66BCD - 1.43BDE + 2.01AC^2 + 2.15BC^2 + 2.14BE^2 - 6.01ABCD + 16.00ABD^2$ (7)

where A = JAS, B = Aluminium oxide, (Al_2O_3), C = temperature, D = particle size, and E = time.

At a confidence level of 95% (Table 4), the terms in the equations are said to be significant when the p-value < 0.05 [27-28]. Accordingly, the terms, AD, AE, BD, BE, ABE, ACD, ACE, BCD, BCE, BDE, $AD^2\,AE^2$, ABC^2, BE^2, $ABCD$ and BDE are significant for char yield with a strong synergic effect.

For bio-oil yield, the terms $ABAE, BC, BE, BCD, BDE, AC^2, BC^2BE^2, ABCD, ABD^2$ are significant. Invariably, particle size is less important to the oil yield in contrast to the temperature and time. The model is also very significant at a p-value < 0.05. Furthermore, the standard deviation (0.77 and 0.96 for char and oil yield, respectively), coefficient of variation R^2 (0.99 and 0.96), R^2_{Adj} (0.97 and 0.89), and other statistical parameters support the accuracy and sufficiency of the models.

Table 3. Experimental Runs and Responses Based on D Optimal Combined Design

Run	A	B	C	D	E	Char yield			Bio-oil yield		
	JAS	Al_2O_3	Temperature (^{0}C)	Particle size (mm)	Time (min)	Actual	Predicted	Residual	Actual	Predicted	Residual
1	95	5	450	2	15	32.1	32.10	0.0040	7.8	7.70	0.0970
2	93	7	450	1	30	33.2	32.89	0.3109	8.4	8.59	-0.1856
3	90	10	450	1	15	29.7	29.44	0.2626	2.4	2.56	-0.1591
4	95	5	650	1	30	26.7	26.92	-0.2226	10.6	10.41	0.1901
5	90	10	560	1	30	26.6	26.72	-0.1214	8.3	8.26	0.0396
6	100	0	450	2	30	33.6	33.28	0.3178	8.6	8.04	0.5611
7	95	5	650	1	15	26.9	26.92	-0.0210	9.3	9.21	0.0924
8	90	10	560	1	22	28	27.91	0.0907	2.7	2.76	-0.0582
9	93	7	460	1	22	25.7	27.12	-1.42	4.4	3.58	0.8178
10	90	10	650	1	23	30.8	29.96	0.8400	8.5	9.08	-0.5826
11	94	6	574	1	23	25.4	25.27	0.1286	3.4	3.05	0.3471
12	100	0	450	1	15	28.2	28.42	-0.2211	4.9	5.22	-0.3231
13	100	0	453	1	22	20.7	20.65	0.0503	6.9	6.64	0.2608
14	95	5	526	2	30	31.8	32.12	-0.3180	5.5	5.40	0.0962
15	95	5	561	1	23	23.9	23.66	0.2431	5.7	5.99	-0.2858
16	95	5	560	1	15	24.5	24.66	-0.1579	2.2	2.27	-0.0720
17	90	10	450	2	30	25.4	25.31	0.0945	1.9	1.94	-0.0406
18	100	0	650	1	15	31.2	31.44	-0.2369	5.4	5.91	-0.0582
19	95	5	560	1	15	24.5	24.66	-0.1579	2.2	2.27	-0.0720
20	95	5	650	2	21	28.7	28.68	0.0188	8.4	8.46	-0.0572
21	100	0	650	2	24	26.8	26.46	0.3396	8.5	7.79	0.7141
22	90	10	455	1	22	31.4	31.65	-0.2484	2.6	2.42	0.1764
23	95	5	450	1	30	27.6	27.31	0.2931	5.8	5.85	-0.0477
24	90	10	650	1	15	27.3	27.68	-0.3795	13.4	7.75	0.2565
25	100	0	650	1	30	20.8	20.98	-0.1818	8.9	9.26	-0.3578
26	95	5	561	1	23	23.9	23.66	0.2431	5.7	5.99	-0.2858
27	95	5	454	1	23	26	25.83	0.1673	1.6	1.90	-0.3044
28	95	5	450	1	15	24.8	24.45	0.3535	5	5.06	-0.0581
29	100	0	524	2	15	38.1	37.70	0.4027	4.2	3.49	0.7064
30	100	0	560	1	22	24.3	23.80	0.5031	6	4.84	1.1600
31	90	10	650	2	25	32.6	32.77	-0.1725	9.8	9.69	0.1142
32	100	0	560	1	30	19.5	19.37	0.1282	6.5	6.32	0.1757
33	90	7	650	1	30	30.1	20.43	-0.3321	15.6	13.18	0.2220
34	100	0	534	2	23	28.5	29.55	-1.05	3.5	5.48	-1.98

35	94	6	574	1	23	25.4	25.27	0.1286	3.4	3.05	0.3471
36	90	10	525	2	15	34.2	34.05	0.1503	2.5	2.62	-0.1179
37	95	5	629	2	30	29.9	29.71	0.1927	8.4	8.67	-0.2672
38	100	0	450	1	30	21.8	22.01	-0.2066	5.6	5.84	-0.2409
39	95	5	650	2	21	28.7	28.68	0.0188	8.4	8.46	-0.0572
40	95	5	454	1	23	26	25.83	0.1673	1.6	1.90	-0.3044

Table 4. ANOVA for the char and oil yields

Source	Sum of Squares	DF	Mean Square	F-value	p-value
Char yield					
Model	620.19	29	21.39	36.36	< 0.0001*
Linear Mixture	54.03	1	54.03	91.86	< 0.0001*
AD	62.32	1	62.32	105.95	< 0.0001*
AE	139.50	1	139.50	237.19	< 0.0001
BD	7.98	1	7.98	13.58	0.0042*
BE	5.82	1	5.82	9.90	0.0104*
ABE	74.68	1	74.68	126.97	< 0.0001*
ACD	9.14	1	9.14	15.53	0.0028*
ACE	22.91	1	22.91	38.96	< 0.0001*
BCD	11.19	1	11.19	19.03	0.0014*
BCE	3.53	1	3.53	6.00	0.0343*
BDE	52.95	1	52.95	90.03	< 0.0001*
AD^2	67.67	1	67.67	115.06	< 0.0001*
AE^2	28.14	1	28.14	47.84	< 0.0001*
BC^2	6.89	1	6.89	11.72	0.0065*
BE^2	3.76	1	3.76	6.40	0.0299*
ABCD	4.34	1	4.34	7.38	0.0217*
ABDE	6.12	1	6.12	10.40	0.0091*
Residual	5.88	10	0.5881	-	-
Lack of Fit	5.88	5	1.18	-	-
Pure Error	0.0000	5	0.0000	-	-

* Significant, Standard deviation = 0.77, mean = 27.63, co-efficient of variation (%) = 2.78, $R^2 = 0.99$, $R^2_{Adj} = 0.96$,

Oil yield

Model	316.39	29	10.93	11.85	0.0001*
Linear Mixture	0.1826	1	0.1826	0.1979	0.0066*
AB	10.02	1	10.02	10.86	0.0081*
AE	8.74	1	8.74	9.48	0.0117*
BC	61.37	1	61.37	66.54	<0.0001*
BE	27.69	1	27.69	30.02	0.0003*
BCD	10.83	1	10.83	11.75	0.0065*
BDE	8.06	1	8.06	8.74	0.0144*
AC^2	7.27	1	7.27	7.88	0.0185*
BC^2	7.96	1	7.96	8.63	0.0148*
BE^2	9.01	1	9.01	9.77	0.0108*
ABCD	6.71	1	6.71	7.28	0.0224*
ABD^2	24.98	1	24.98	27.09	0.0004*
Residual	9.22	10	0.9223	-	-
Lack of Fit	9.22	5	1.84	-	-
Pure Error	0.0000	5	0.0000	-	-

*Significant, Standard deviation = 0.96, mean = 5.92, Co-efficient of variation (%) = 16.22, R^2 = 0.97, R^2_{Adj} = 0.89

Having obtained accurate models, the experimental data points were predicted and compared (Fig. 2a and b). Accordingly, most of the data lie nearly to the straight line with R^2 of about 1, suggesting excellent concord between the model response and experimental data. Invariably, the models can be used to predict the value of char and oil yields.

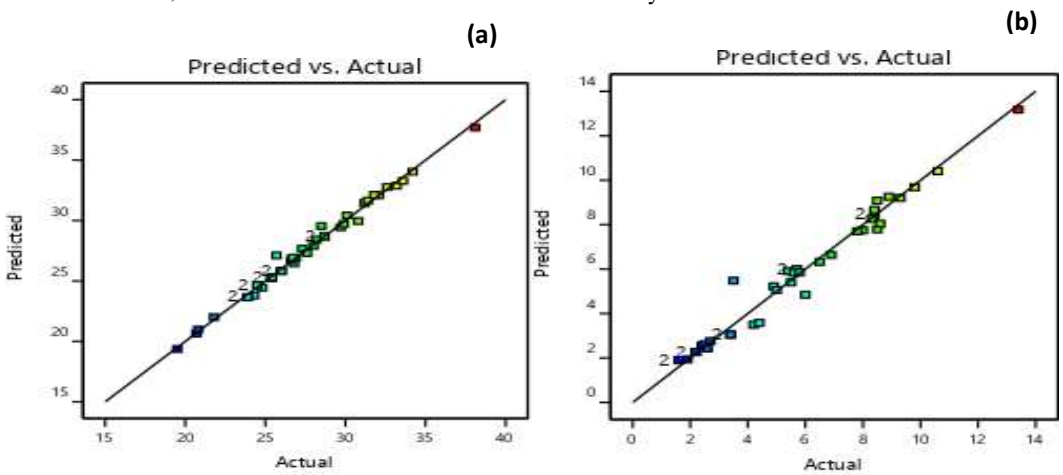

Fig. 2. Comparison of actual and forecasted values of the responses for (a) char yield, (b) oil yield

Influence of process conditions on the bio-oil yield

The impacts of the two mixture components (Jatropha curcas, Aluminium oxide (Al_2O_3)) and the residence time factor, temperature and particle size on the oil yield of the fuel are illustrated in Fig. 3 a-c. According to the 3-D plots, higher pyrolytic temperature up to (650 ^{0}C) and volume of JAC at 7 wt.% alumina favoured bio-oil production. For instance, 15.6 % bio-oil yield was obtained at 650 ^{0}C compared to 8.4% at 450 ^{0}C. Similarly, increased pyrolysis duration from 15 to 30 min raised the bio-oil yield by 46.2 % and reduced solid residue by 12.5%. The decrease in the solid yield may be attributed to the loss of energy-lean components or formation of energy-rich components (Bach and Lee, 2017) while the increase in the oil yield may be due to the influence of catalyst (Ahmad et. al., 2019). According to the 3-D plots, the interaction between temperature and time, at constant values of jatropha curcas, Al_2O_3 and particle size, illustrated immense effects of these parameters on the oil yield. The bio-oil yield of the mixture fuel significantly increased to 15.6 % upon increase of alumina fraction from 5 up to 7 wt.% and decrease of JAC fraction from 95 to 93 wt.% at 650 ^{0}C, 1 mm particle size and at residence time of 30 min (Fig. 3a-c).

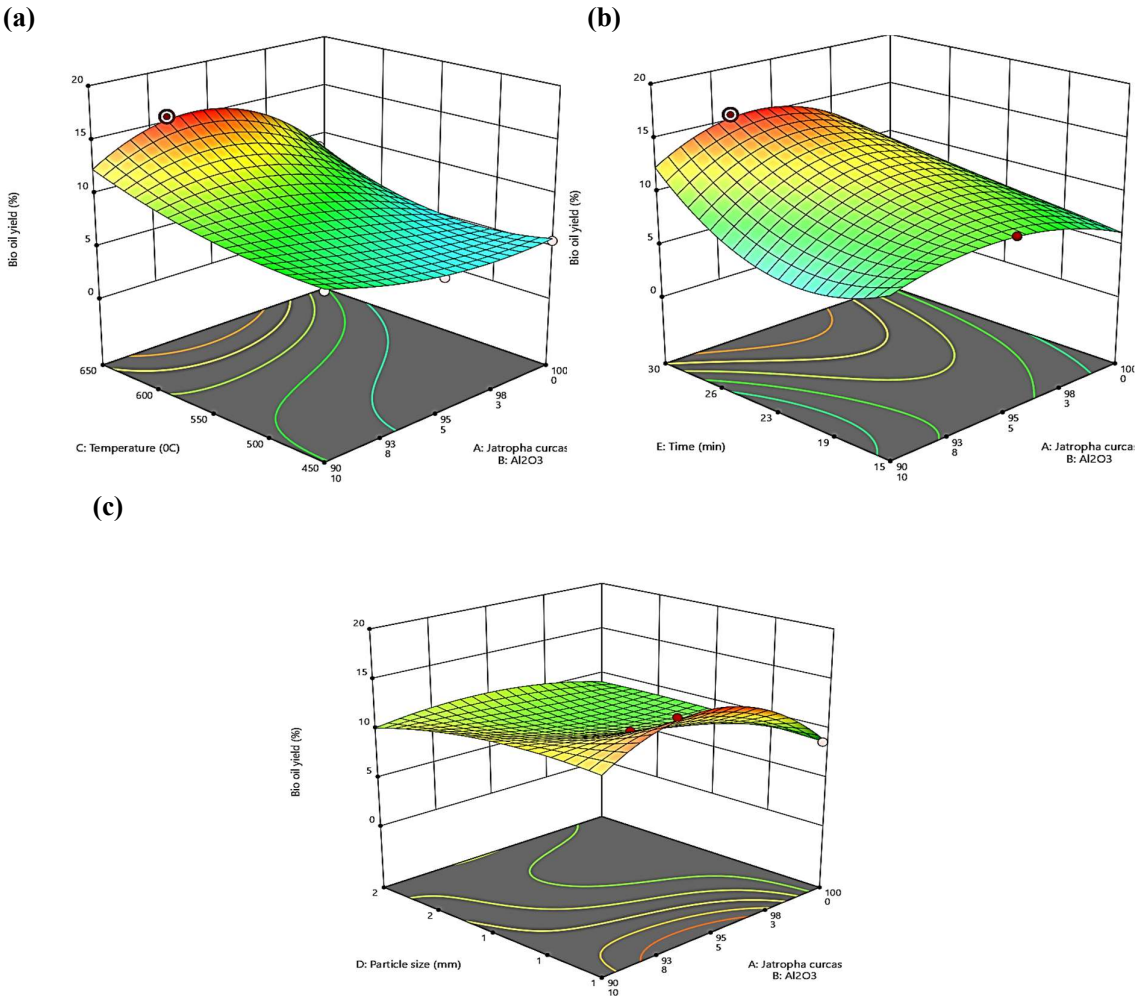

Fig 3: 3D response surface plot for the mutual interaction between the JAS-alumina catalyst mixture at different temperature, time, and particle size

BIO-OIL AND CHAR CHARACTERIZATION

Scanning Electron Microscopy (SEM) analysis of char and bio-oil yield without and with attendance of catalyst (Fig. 4 a-c) indicated that the surface of the biochar was cracked with honeycomb pore structure at the same operating conditions, temperature (650 ^{o}C), particle size (1 mm) and residence time of (30 mins). The pores present on the surface of the biochar may make it applicable in the adsorption process (Kumar et. al., 2019 and Oladosu et. al., 2022). From experimental results, Run 33 [93:7, 650 °C, 1 mm and 30 mins] gave optimum oil yield (15.6 %) while Run 25 [100:0, 650 °C, 1 mm and 30 mins] gave relatively average oil yield (8.9 %) (Fig. 4c). It was also acknowledged that the carbon content of the JAS catalyst mixture was enhanced (67.8%) for Run 33 in comparison to Run 25 (53.4 %) while the oxygen gets reduced (7.5%) as against (18.6%) without the presence of a catalyst. Moreover, the presence of a catalyst boosts the calorific value (43.5 kJ/kg) than without a catalyst (38.1 kJ/kg) because of an increase in elemental composition. The results indicated that Run 25 has a higher viscosity (74.93 cSt) which is a key disadvantage of its application in the automobile industry. However, the addition of 7 wt % Al_2O_3 to the mixture considerably drops the viscosity to 48.5cSt (Table 5)

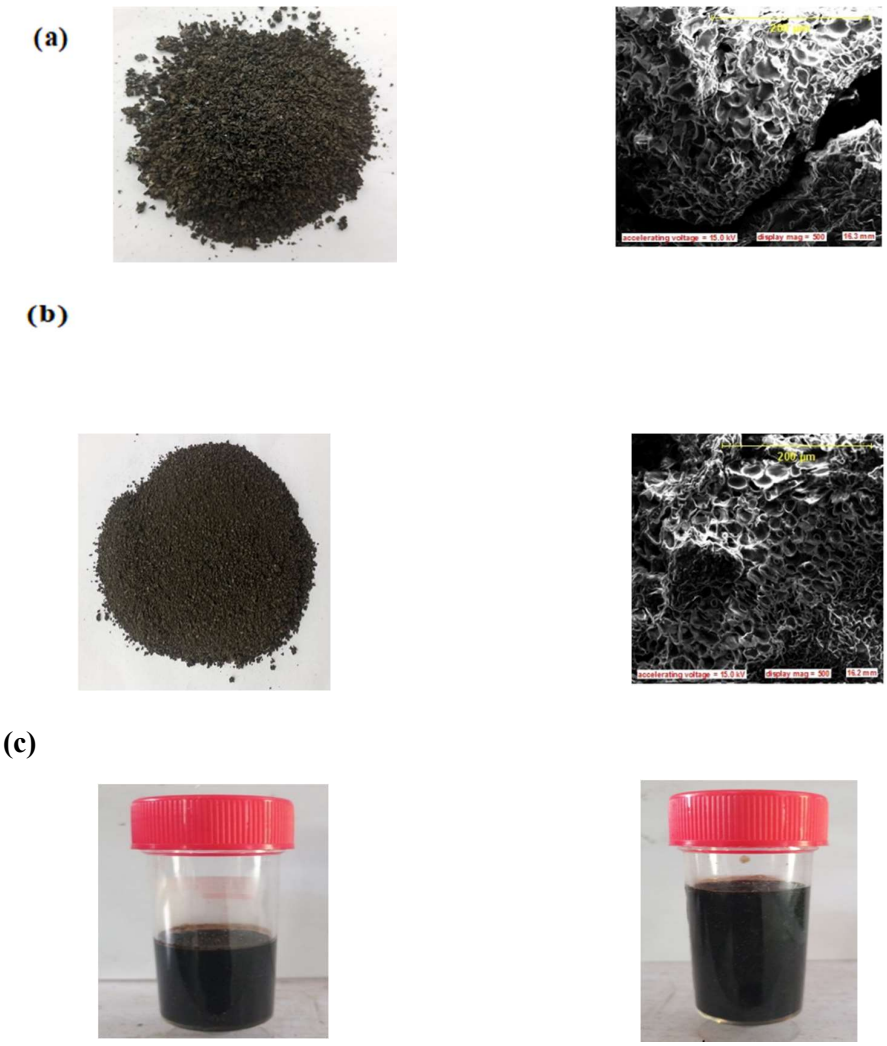

Fig. 4. Biochar (SEM) analysis of *Jatropha curcas and* bio-oil yield (a) without catalyst (b) with the catalyst and (c) bio-oil yield at the same process condition

Table 5: Properties of Fuel catalyst mixture at the optimized conditions

Analysis	93:7; 650 ^{0}C, 1mm 30mins	100:0; 650^{0}C, 1mm 30 mins
Carbon %	67.8	53.4
Hydrogen %	6.3	4.8
Oxygen	7.5	18.6
Nitrogen %	1.8	2.2
Sulphur%	0.63	1.53
Calorific Value kJ/kg	43.5	38.1
Moisture	3.8	4.93

FTIR Analysis of Bio-oil yield

The absorption band, 3171.46 – 344.19 cm^{-1}, in the FTIR spectra (Fig 5) is linked with the hydroxyl group (OH) showing the existence of phenols, water, protein, alcohol, and aromatic compounds. Furthermore, the noticeable peak at 2924 cm^{-1} is connected to the C-H extending bond. The occurrences of alkanes were seen at the highest 2850 cm^{-1} while the topmost 1701 cm^{-1} showed the presence of ketone, aldehyde, and carboxylic acid as a result of the widening vibration of C=O (Singh et al. 2020). The peak at 1400 cm^{-1} displayed the presence of alkanes because of the occurrence of C-H bending vibration. Other peaks at 966, 722, and 667 cm^{-1} confirmed the appearance of perfumed products in the pyrolytic liquid. The appearance of the aliphatic and slight aromatic inveterate the presence of lignin, cellulose, and hemicellulose which could be useful for numerous applications

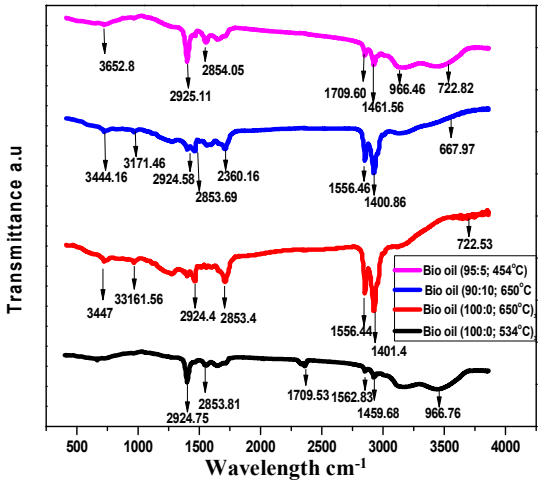

Fig. 5 FTIR of Catalyst Oil

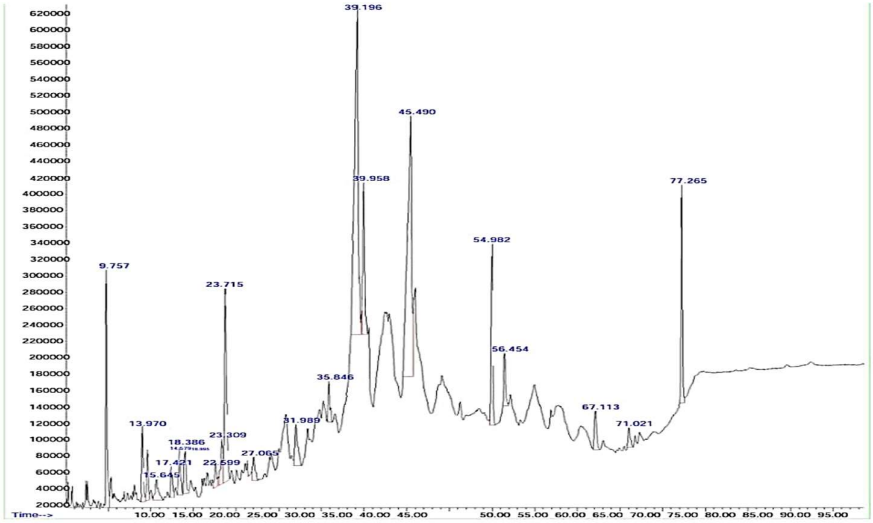

Fig. 6. GC-MS analysis

Table 6 Major chemical compounds in the optimized bio-oil yield sample classified by GC–MS.

Compounds	Area (%)
5-Isothiazolecarboxamide	6.11
2-Propenal, 3-(dimethylamino) –2– (methylamino) –	
1,3–Dimethy-4,5 (1H) – dihydro-1, 2,4-triazole-5-one	
Methane, iodo-	2.13
Methylthiouracil	
5-Amino-1-methyl-4-nitropyrazole	
3,3,5-Trimethylhexahydraozepine, N-acetyl-	1.53
3-Chloro-6-diazocyclohexa-2, 4-dienone	
Magnesium, bis (.eta.<5>-2, 4-cyclopentadien-1-yl)-	
Butanoic acid, 2-bromo-, methyl ester	1.46
2-t-Butyl-6-(2-hydroxy-2-napthalen-1-yl-ethyl) – [1,3] dioxin-4-one Butanoic acid, 2-bromo-, methyl ester	
Boroxine, diethyl methyl-	0.99
Biphenyl	
3-Quinolinecarbonitrile	
Tetracyclo [5.2.1.0 (2,6).0 (3,5)] non-8-ene, 4-methyl-4-phenyl-, endo Naphthalene, 1,7-dimethyl-	2.10
Naphthalene, 1,4-dimethyl-	
Pent-1-yn-3-ene, 4-methyl -3-phenyl	
Benzamine, 2-methoxy-4-nitro-	1.77

Pyrimidine, 2-(dimethylamino)-5-nitro-	
Diphenylmethane	
3-Phenylbicyclo [3.2.1] octa-2, 6-diene	1.01
3-Phenylbicyclo [3.2.1] octa-2, 6-diene	
2,3,4-Trimethoxyphenylethylamine	
Phenol, 2,4-bis (1,1-dimethylethyl)	1.85
Phenol, 2,4-bis (1,1-dimethylethyl)	
Benzophenone	
1,1'-Biphenyl. 3,4'-dimethyl-	8.57
Pyrido [2,3-b] iodole, 6-methyl-	
2H-Pyran-5-carboxylic acid, 4-methoxy-6-methyl-2-oxo-, ethyl ester	
1H-Pyrazole, 4-chloro-1-phenyl-	1.08
Phenanthrene	
1-Cyclohexene, 4,4-dimethyl-1-[(trimethylsilyl)oxy]-	
Naphthalene, 2,3-dimethyl-	2.43
Naphthalene, 2,3-dimethyl-	
4-Chloro-6- (2-hydroxyphenyl) pyrimidine	
Benzoic acid, m-[[(dimethylamino) methylene] amino]-, methyl ester	1.39
Pyrene, 4,5,9,10-tetrahydro-	
4,4'-Dimethoxy-2,2'-dimethylbiphenyl	
Imidazole, 2-[4-methoxyphenyl]-4-triflouromethyl-	23.71
1-[3,4,5-Trimethoxyphenyl] thiourea	
2-[p-Chlorophenyl] pyrolidine	
6-Chlorochromone	5.47
.alpha.-(p-Methylphenyl) benzyl acetate	
1,2,3-Trimethoxybenzene	
Benzene, 1,3-dinitro-	22.83
1 (2H) –Acenaphthylenone	
Benzenemethanol,.alpha.-methyl-.alpha.-phenyl-	
dl-4-Ethyl-5-methyl-3-(1-carboxyethyl)-.delta. (4)-thiazoline-2-thion	5.07
Furan-2-carbaldehyde, 5-(4-methyl-3-nitrophenyl)-	
2-Propenoic acid, 2-cyano-3-(4-methoxyphenyl)-, ethyl ester	
2-Acetyl-3-(1-methyl-2-pyrrolyl)-1, 4-benzenediol	1.87

N-(2-Acetylcyclopentylidene)-p-antisidine	
4-(1H-[1,2,4] Triazole-3-carbonyl)-piperazine-1-carboxylic acid ethyl ester	
3,5-Dimethyl-1-dimethylvinylsilyloxybenzene	1.77
Pyridine-4-carboxylic acid, 1,2-dihydro-3-cyano-5, 6-dimethyl-2-oxo-, methyl ester	
1-(3,6,6-Trimethyl-1,6,7,a-tetrahydrocyclopenta[c] pyran-1-yl) ethanone	
	0.89
	5.99

The organic compounds existing in the pyrolytic liquid were recognised by the GC-MS analysis (Fig. 6 and Table 6). Accordingly, the bio-oil contained predominantly pyrimidine (23.71%), pyrrolidine (22.83%), and phenols (~8.57%). These compounds are largely obtained from hemicellulose decomposition (Chukwuneke et. al., 2021). By-products of benzoic acid and esters (dimethylamino) were also gotten in large quantities. The liquid products contain chemicals with oxygen-holding functional groups. Oxygen-containing chemicals can be produced from fossil fuels using hydration or oxygenation of the olefins to present oxygen-containing functional groups. These functional groups are available in the liquid part obtained during pyrolysis (Chukwuneke et. al., 2021). The outcomes revealed that bio-oil produced from the Jatropha caucus possessed a vast quantity of preservatives such as phenols, alcohols, acids, and others. Therefore, the efficacy of JAS could be used to produce biofuels and value-added chemicals.

3.7 Optimization of ANN Architecture

The pyrolysis results were also modelled through ANN and the outcomes were likened to those of OD. The optimum ANN architecture considered was the one with the minimum value of MSE and the maximum value of R^2. To achieve optimal architecture for training the hidden layers, *trainlm*, *trainscg*, and *trainbr* algorithms were considered. The most satisfactory results were obtained with the '*trainlm*' algorithm. Table 7 presents some of the best performing combinations of different values of training: validation: test data division ratios with hidden layers for the *trainlm* algorithm. At length, 15 hidden layers with 70:15:15 ratio was optimum for the bio-oil yield prediction. Accordingly, the best ANN architecture has the least MSE (2.15e-05) and the largest R^2 (0.9639).

There is a non-linear relationship between the number of hidden layers and the data division ratio as a comparison of the model performance for the bio-oil yield from serial number 1 to 7 (Table 7). Going from 1 to 2, it seems that increasing the training data percentage while keeping the number of hidden layers constant improves upon the MSE and R^2 values. From 2 to 3, however, increasing the number of hidden layers with a constant division ratio result in less desirable values of R^2 and MSE. Interestingly, a further increment on the hidden layer (from serial number 3 to 4) while keeping the division ratio constant eventually provides a better performance of both MSE and R^2. While keeping hidden layers constant, a slight upward change in the validation data ratio at the expense of only the test data ratio has no effect on the R^2 value but a slight

penalty on the MSE (from serial number 4 to 5). The R^2 value remains unchanged with a downward review of the training data division at constant validation data ratio and number of hidden layers (from serial number 5 to 6). In a contrast, the bio-oil yield model benefits the most from lower training data ratio and hidden layers in serial number 7.

Table 7 ANN architecture

S/N	Data division ratio (%)	Number of hidden layers	MSE	R^2
		Bio-oil yield		
1	70:15:15	10	9.03e-05	0.9335
2	80:10:10	10	8.43e-05	0.9353
3	80:10:10	20	2.00e-04	0.8953
4	80:10:10	25	1.17e-04	0.9134
5	80:15:5	25	2.27e-04	0.9134
6	70:15:15	25	7.20e-05	0.9134
7	70:15:15	15	2.15e-05	0.9639

The performance of the optimum ANN architectures are depicted in Fig. 7. The regression coefficients for the training and testing datasets (0.9995 and 0.9639) and the number of epochs (9) establish the reliability of the model. The error bound plot (Fig 7d) shows that most of the errors are ranged from ±0.02363. The ANN model training state (Fig 7e) and a cross-plot of the predicted values with the actual values (Fig 7f) present the accuracy of the model.

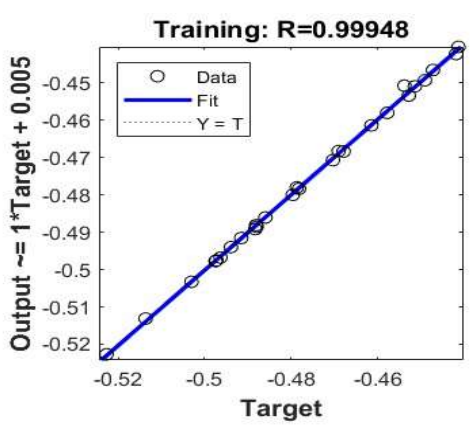

(a)

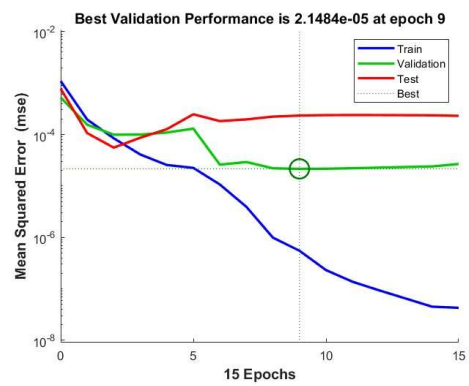

(b)

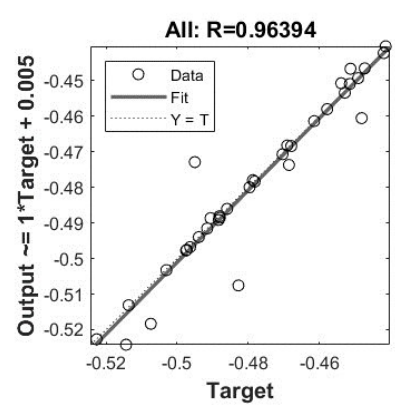

(c)

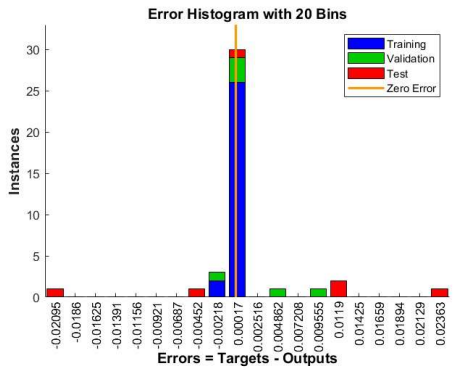

(d)

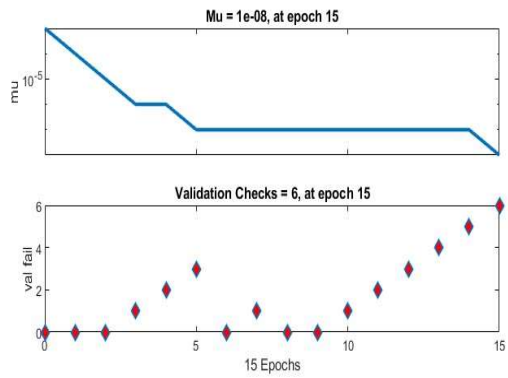

(e)

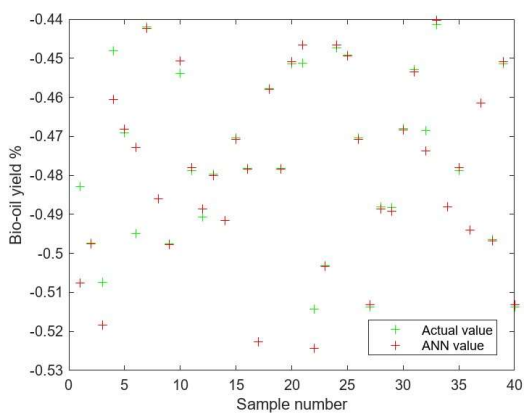

(f)

Fig. 7: Results of the ANN model for bio-oil yield. (a) The training dataset, (b) Performance, (c) Error histogram, (d) Regression, (e) Training state, and (f) Actual and ANN values of bio-oil yield.

CONCLUSIONS

This study deals with the optimization and prediction of bio-oil yield from catalytic pyrolysis of *Jatropha curcas* seeds in a fixed bed reactor. The maximum bio-oil yield of 15.6 wt. % was obtained at an operating condition of 650 ^{0}C temperature, 30 min time, and 1 mm particle size. The Correlation Coefficient (R^2) of the model for the bio-char and bio-oil yield under the OD were 0.998 and 0.996, respectively. The optimized ANN architecture employed the in-built Levenberg-Marquardt training algorithm in MATLAB. Random division of the data into training, validation and testing sets followed 70:15:15 percentage proportions with 15 hidden layers. This resulted in the minimum Mean Square Error (MSE) of 2.15e-05 and Correlation Coefficient (R^2) of 0.96394 for the bio-oil yield.

The bio-oil yield contains phenols, ketone, aldehyde, carbonyl/carboxylic acid, pyrimidine, and pyrrolidine derivatives with phenol acid and isothinazole carboxamide derivatives being on the lower side. The prediction accuracy indicates that both ANN and OD can be deployed for the accurate prediction of bio-oil in biomass pyrolysis. The analysis of this bio-oil shows that it has the potential to be a source of bioenergy and biochemical capabilities. Further study can be carried out to extract some useful chemicals from the liquid products and non-condensable gas.

Declaration of Competing Interest: The authors affirm that they have no competing financial interests or personal affairs that could have acted to influence the work reported in this paper.

REFERENCES

Adeniyi, A.G., Abdulkareem, S.A., Ighalo, J. O. (2021). Thermochemical Co-conversion of Sugarcane Bagasse-LDPE Hybrid Waste into Biochar. *Arab. J. Sci. Eng.* **46,** 6391–6397.

Ahmad, I., Ali, N.,Qadir, A., Shahzad, K., Saleem, M. (2018) Effect of catalyst (aluminum oxide) on bio-oil yield from pyrolysis of pakistani

cotton stalk. *Journal of the Pakistan Institute of Chemical Engineers***46** (1), 23–34.

Ahmad, T. Y., Muslikhin, H., Ahmad, A. F; Prasasti, W.P., Cornelius, T. K. (2019) Preparation and characterization of bio-coal briquettes from pyrolysed biomass-coal blends. *Journal of Engineering Science and Technology***14**, 3569–3581.

Antwi, P., Li, J., Opoku, P., Meng, J., Shi, E., Deng, K., Bondinuba, F.K. (2017) Estimation of biogas and methane yields in a UASB treating potato starch processing wastewater with backpropagation artificial neural network Biogas Gas meter Water lock Effluent. *Bioresource Technology***228**, 106–115.

Arulprakasajothi, M., Beemkumar, N., Parthipan, J., Battu, N. (2020)Investigating the physio-chemical properties of densified biomass pellet fuels from fruit and vegetable market waste. *Arab. J. Sci. Eng.***45**, 563–574.

Asafa, T.B., Tabet, N, Said, S.A.M. (2013) Neurocomputing Taguchi method – ANN integration for predictive model of intrinsic stress in hydrogenated amorphous silicon film deposited by plasma-enhanced chemical vapour deposition. *Neurocomputing***106**, 86–94.

Bach, Q., Lee, C. (2017) Process modeling and optimization for torrefaction of forest residues. *Energy***138**, 348-354.

Boubacar Laougé, Z., Çığgın, A. S., Merdun, H. (2020) Optimization and characterization of bio-oil from fast pyrolysis of Pearl Millet and Sida cordifolia L. by using response surface methodology. *Fuel***274**, 117842.

Chen, W. H. Lin B. J., Lin Y.Y.,Chu, Y., Ubando, A.T., Show, P.L., Ong, H.C., Chang, J., Ho, S., Culaba, A.B., Pétrissans, A., Pétrissans, M. (2021) Progress in biomass torrefaction: Principles, applications and challenges. *Prog. Energy Combust. Sci.***82**, 100887.

Chukwuneke, J.L., Orugba, H.O., Olisakwe, H.C., Chikelu, P.O.(2021) Pyrolysis of pig-hair in a fixed bed reactor: Physico-chemical parameters of bio-oil. *South African J. Chem. Eng.***38,** 115–120.

David, G.F., Justo, O.R., Perez, V.H., Garcia-Perez, M.(2018) Thermochemical conversion of sugarcane bagasse by fast pyrolysis: High yield of levoglucosan production. *J. Anal Appl. Pyrolysis***133**, 246–253.

Eriola, B., Ezekiel, T. (2015) Modelling and optimization of bioethanol production from breadfruit starch hydrolysate vis-à-vis response surface methodology and artificial neural network. *Renewable Energy***74**, 87-94.

Garba, M.U., Musa, U., Olugbenga, A.G., Mohammad, Y.S., Yahaya, M., Ibrahim, A.A. (2018) Catalytic upgrading of bio-oil from bagasse: Thermogravimetric analysis and fixed bed pyrolysis. *Beni-Suef Univ. J. Basic Appl. Sci.***7**, 776–781.

Guedes, R.E., Luna, A.S.,Torres, A. R. (2018)Operating parameters for bio-oil production in biomass pyrolysis: A review. *J. Anal. Appl. Pyrolysis***129**, 134–149.

Jeirani, Z., Mohamed, J. B., Ali, B. (2012) The optimal mixture design of experiments: Alternative method in optimizing the aqueous phase composition of a microemulsion. *Chemom. Intell. Lab. Syst.***112**, 1–7.

Kamoru O. Oladosu, Simeon A. Babalola, Rasaq K. Ajao & Mutiu F. Erinosho (2024) Torrefaction of Bambara Groundnut Shell: experimental optimization and prediction of the energy

conversion efficiency using statistical and machine learning approaches, *International Journal of Ambient Energy*, 45:1, 2277309

Kanaujia, P.K., Naik, D.V., Tripathi D.,Singh, R., Poddar, M.K., Konathala, L.N.S., Sharma, Y.K. (2016) Pyrolysis of Jatropha Curcas seed cake followed by optimization of liquid-liquid extraction procedure for the obtained bio-oil. *J. Anal. Appl. Pyrolysis***118**, 202–224.

Kanwal, S., Chaudhry, N., Munir, S., Sana, H. (2019) Effect of torrefaction conditions on the physicochemical characterization of agricultural waste (sugarcane bagasse). *Waste Manag.***88**, 280–290.

Kareem, Buliaminu, Kamoru O. Oladosu, Abass O. Alade, and Mondiu O. Durowoju (2018). " Optimization of Combustion Characteristics of Palm Kernel-Based Biofuel for Grate Furnace." *International Journal of Energy and Environmental Engineering* 9 (4): 457–472.

Kethobile, E., Ketlogetswe, C.,Gandure, J. (2020) Torrefaction of non-oil Jatropha curcas L. (Jatropha) biomass for solid fuel. *Heliyon***6** (12), e05657.

Kumar, R., Strezov, V., Lovell, E., Kan, T., Weldekidan, H., He, J., Dastjerdi, B., Scott, J. (2019)Bio-oil upgrading with catalytic pyrolysis of biomass using Copper/zeolite-Nickel/zeolite and Copper-Nickel/zeolite catalysts. *Bioresour. Technol.***279**, 404–409.

Lewis, A.D.,Fletcher, T.H.(2013)Prediction of sawdust pyrolysis yields from a flat-flame burner using the CPD model. *Energy and Fuels***27**, 942–953.

Mishra, R.K., Mohanty, K. (2020) Effect of low-cost catalysts on yield and properties of fuel from waste biomass for hydrocarbon-rich oil production. *Materials Science for Energy Technologies***3**, 526–535.

Mishra, R.K., Muraraka, A., Mohanty, K. (2020) Optimization of process parameters and catalytic pyrolysis of Cascabela Thevetia seeds over low-cost catalysts towards renewable fuel production. *Journal of the Energy Institute***93**, 2033–2043.

Mth, N. Mubarak, N. M. (2019) Characterization and process optimization of biochar produced using novel biomass, waste pomegranate peel: A Response Surface Methodology Approach. *Waste and Biomass Valorization***10**, 521–532.

Ndukwu, M.C., Horsfall, I.T., Ubouh, E.A., Orji, F.N., Ekop, I.E., Ezejiofor, N.R.(2021) Review of solar-biomass pyrolysis systems: Focus on the configuration of thermal-solar systems and reactor orientation. *J. King Saud Univ. - Eng. Sci.***3**, 413–423.

Okonkwo, U.C., Onokpite, E., Onokwai, A.O. (2018) Comparative study of the optimal ratio of biogas production from various organic wastes and weeds for digester/restarted digester. *J. King Saud Univ. - Eng. Sci.***30**,123–129.

Oladosu, K.O., Asafa, T.B., Erinosho, M. (2021) Artificial neural network prediction of CO emission and ash yield from co-combustion of empty fruit bunch, palm kernel shell and kaolin. *Environmental Science and Pollution Research***28**, 42596–42608.

Oladosu, Kamoru, Ayodeji Olawore, Abass Alade, and Maruf Kolawole (2022). "Optimization of Hhv and Energy Yield from Torrefaction of Albizia Zygia Wood- Calcium Hydrogen Phosphate Catalyst Blends Using Optimal Combined Design." *Acta Periodica Technologica* (53): 109‑122.

Ozonoh, M., Oboirien, B., Daramola, M.O. (2020) Optimization of process variables during torrefaction of coal/biomass/waste tyre blends: Application of artificial neural network & response surface methodology. *Biomass and Bioenergy***143**, 105808.

Rahman, M.M., Nishu, S.M., Chai, M., Li, C., Liu, R., Cai, J. Potentiality of combined catalyst for high-quality bio-oil production from catalytic pyrolysis of pinewood using an analytical Py-GC/MS and fixed bed reactor. *J. Energy Inst.***93**,1737–1746.

Siddiqui, M.T.H., Nizamuddin, S., Mubarak, N.M., Shirin, K., Aijaz, M., Hussain, M., Baloch, H.A. (2019). Characterization and process optimization of biochar produced using novel biomass, waste pomegranate peel: A Response Surface Methodology approach. *Waste and Biomass Valorization***10**, 521–532.

Singh, R. K., Chakraborty, J. P., Sarkar, A. (2020) Optimizing the torrefaction of pigeon pea stalk (Cajanus cajan) using response surface methodology (RSM) and characterization of solid, liquid and gaseous products. *Renew. Energy***15**, 677–690.

Sunarno, S., Rochmadi, R., Mulyono, P., Aziz, M., Budiman,A. (2018) Kinetic study of catalytic cracking of bio-oil over silica-alumina catalyst. *BioResources***13**, 1917–1929.

Tian, X.,Dai, L.,Wang, Y.,Zeng Z., Zhang, S., Jiang, L., Yang,X., Yue, L., Liu,Y., Ruan, R. (2020)Influence of torrefaction pretreatment on corncobs: A study on fundamental characteristics, thermal behavior, and kinetic. *Bioresour. Technol.***297**, 122490.

Wang, Q., Zhang, X., Sun, S., Wang, Z., Cui, D. (2020) Effect of CaO on Pyrolysis Products and Reaction Mechanisms of a Corn Stover. *ACS. Omega***5**,10276–10287.

Yusuff, A.S., Owolabi, J.O. (2019) Synthesis and characterization of alumina-supported coconut chaff catalyst for biodiesel production from waste frying oil. *South African J. Chem. Eng.***30**, 42–49.